


Effective single-electron treatment of ion collisions with multielectron targets without using the independent-event model

I. B. Abdurakhmanov ^{*}, C. T. Plowman , K. H. Spicer , I. Bray , and A. S. Kadyrov [†]

Curtin Institute for Computation and Department of Physics and Astronomy, Curtin University, GPO Box U1987, Perth, WA 6845, Australia

 (Received 7 January 2021; revised 26 July 2021; accepted 11 October 2021; published 29 October 2021)

In ion-atom collisions involving multielectron targets the role of inner-shell electrons becomes important with increasing collision energy. Usually, processes involving the outer-shell and inner-shell electrons are treated using an independent-event model. However, the independent-event model becomes impractical when the number of shells is more than two. We develop an effective single-electron approach to ion collisions with multielectron atomic targets that overcomes this difficulty by treating all the atomic electrons on an equal footing. The approach allows the calculation of single-ionization and single-electron transfer cross sections by including the excitation of any one of the inner- or outer-shell target electrons. Accordingly, the approach does not differentiate which one of the many target electrons is captured or ionized. This is a unique feature of the proposed approach. The ground-state wave function for the target atom obtained in the multiconfiguration Hartree-Fock approach is used to calculate the probability density for the whole atom. The latter is then averaged over the spatial coordinates and spin variables of all of the target electrons except for the position of one electron from the nucleus. The obtained single-electron probability density is then used to derive a pseudopotential describing the interaction of one electron with an effective field produced by the target nucleus and the other electrons. The procedure reduces the many-body Schrödinger equation governing the collision system effectively into a three-body one. The reduced Schrödinger equation is solved using the two-center wave-packet convergent close-coupling approach. As an illustrative example we calculate integrated cross sections for single-electron transfer and ionization in proton collisions with lithium, sodium, and potassium. The results obtained agree very well with available experimental data for electron transfer. However, we find significant discrepancies with experiment for single ionization of Na and K, which warrant further experimental and theoretical investigations.

DOI: [10.1103/PhysRevA.104.042820](https://doi.org/10.1103/PhysRevA.104.042820)

I. INTRODUCTION

Ion-atom collisions represent one of the important topics in atomic physics due to applications that benefit from a quantitative understanding of such collisions. Solar wind problems in astrophysics [1], plasma modeling for fusion energy [2,3], and hadron therapy of cancer [4] are just some of the examples. The recent progress in energetic ion-atom and ion-molecule collisions has been given in Ref. [5].

From the viewpoint of theoretical studies of ion-atom collisions, modeling bare ion-hydrogen collisions represents the simplest, but still formidable, challenge since it is a genuine three-body problem where the interactions between all of the particles and the two-body bound-state wave functions in the reaction channels are analytically known. For this reason, it has served as a test bed for the development of several theoretical models based on the molecular-orbital close-coupling [6], atomic-orbital close-coupling [7–9], the basis generator method [10], the numerical lattice method [11–13], the continuum distorted-wave method [14–16], the classical trajectory Monte Carlo method [17,18], and various perturbative methods [19]. Recent developments in the field

include quantum-mechanical and semiclassical implementations of the convergent close-coupling method [20–22].

The next collision system in a sequence of complexity is fully stripped ion scattering on a two-electron target of helium. This system is also considered to be the simplest one which includes physics associated with the correlation of the target electrons. The problem has been thoroughly studied in a number of theoretical works, see, e.g., Refs. [23–25] and references therein.

Collision systems with one- or two-electron targets can be dealt with in an *ab initio* manner without significant approximations. However, as the number of target electrons increases it becomes unavoidable to introduce approximations to the problem. Depending on the electronic structure of the target there already exist several types of approximations. For instance, proton scattering on atomic targets with only one electron in the valence shell (e.g., alkali-metal atoms) is usually reduced effectively to the three-body problem by modeling the interaction potential of the target inert core with the valence electron and the incident proton. With these modifications, the formalism developed for the proton-hydrogen collision problem can then be utilized. In collision systems where the target atom has two valence electrons (e.g., alkaline-earth atoms) or a closed shell (e.g., inert gases), usually there is a strong influence of electron-electron correlation and electron-exchange effects. Such collision systems can be

^{*}ilkhom.abdurakhmanov@curtin.edu.au

[†]a.kadyrov@curtin.edu.au

treated using the models based on the formalism developed for proton-helium collisions where there are the necessary ingredients to take these effects into account.

The quality of modeling the effective potential plays a crucial role in the accurate description of the collision system. In collisions involving targets with more than one electronic shell, excitation of inner-shell electrons can have a considerable effect on reaction cross sections even for single electron processes, such as single electron excitation, and ionization and single electron capture. However, models which assume a frozen inert core of the target completely neglect this effect.

Despite significant progress in ion-atom collision theory, due to the complicated electronic structure of multielectron atoms, modeling proton collisions with such targets still remains challenging. Many theoretical approaches resort to empirical modeling of the interaction potentials between the participants of the reaction. Such approaches are usually limited to the description of a specific collision process which is being investigated. In particular, in ion-atom collisions involving multielectron targets, the role of inner-shell electrons becomes important with increasing collision energy. Usually, the contributions of the outer and inner-shell electrons are taken into account using an independent-event model, where processes involving the outer-shell and inner-shell electrons are artificially separated and treated independently. However, the independent-event model becomes cumbersome and impractical when the number of shells is more than two. Furthermore, often the independent-event model fails, e.g., when it is applied to double ionization of He [23,25].

As an example of ion collisions with multielectron targets, in this work we consider proton scattering on alkali-metal atoms. A large amount of experimental data [26–41] for proton scattering on Li, Na, and K has been collected for integrated electron-capture and excitation cross sections. These measurements for single electron capture and single electron ionization only detect an electron without specific information whether it originated from the outermost or inner shells of the target.

Early investigations into proton collisions with alkali atoms were conducted by Stary *et al.* [42] using an optical-potential method. An alternative approach using a continuum-distorted-wave eikonal-initial-state (CDW-EIS) model was developed by McCartney and Crothers [43]. Both of these approaches investigated collision scenarios with projectile energies greater than 1 keV. Dubois *et al.* [44] used the atomic-orbital close-coupling approach to investigate differential cross sections, alignment, and orientation effects for electron capture in proton-Na collisions. More recently Lühr and Saenz [45] investigated single electron loss by alkali atom targets for a wide range of proton projectile energies ranging from 0.25 to 1000 keV. Their method involved a time-dependent coupled-channel approach which treated the alkali targets as one-electron atoms by generating a set of pseudostates for the alkali's valence electron. These pseudostates used a Klapisch model potential [46] to simulate the interaction between the atom's active electron and its frozen-core pseudonucleus. The pseudostates were then expanded using *B*-spline functions to form a set of coupled equations. While good agreement was found between the obtained results and those presented by McCartney and Crothers, notable discrepancies were seen

when compared with the results of Stary *et al.* Lühr and Saenz suggested that an underlying assumption or scaling factor had incorrectly influenced the results of Stary *et al.* or that the presented results had yet to reach full convergence. Another time-dependent channel-coupling approach was developed by Pindzola *et al.* [47]. Differing from Lühr and Saenz, this investigation used frozen Hartree-Fock potentials to generate the pseudostates. For the considered projectile energy range (1 to 100 keV), good agreement was found between their results and those presented by Lühr and Saenz. However, all these theoretical studies were not successful in producing accurate total cross sections for single-electron capture at intermediate to high collision energies. The conclusion was that, at these energies, the incident proton is more likely to capture the electron from the inner shells of the atom rather than the valence electron.

Very recently, we have developed a simple method to calculate electron-transfer cross sections based on one-center close-coupling equations where only target-centered pseudostates are used. The developed method was applied to investigate proton scattering on the lithium atom [48]. The obtained results for the total electron-capture and the $2s \rightarrow 2p$ excitation cross sections were found to be in good agreement with available experimental data. However, this approach cannot provide as much collision information as the genuine two-center approach can. Specifically, there are two shortcomings of this approach. First, it is based on the frozen-core approximation, meaning that the projectile can capture only the valence electron. As mentioned above, in practice as the projectile energy grows, capture of the core electrons gradually become dominant. The approach accounts for this process using the independent-event model. This separation appears to work well in this case but it is artificial and may not work for other targets where the ionic core is not well separated and the frozen-core approximation is not applicable. Additionally, detailed differential studies of the processes occurring during the collision are impossible within this approach.

In the present work our aim is to develop a general approach to fully stripped ion scattering on multielectron atom (ion) targets that have a quasi-one-electron configuration. The approach effectively takes into account the presence of all the particles of the collision system but, at the same time, maintains the number of degrees of freedom of the system low to make calculations feasible. Time-dependent density-functional theory (TDDFT) (see, e.g., Refs. [49–54] and references therein) is another example of nonperturbative approaches to ion collisions with multielectron targets. Our method is an approximation and it is not as rigorous as the time-dependent density-functional theory. However, it can serve a simpler alternative to TDDFT in cases where our approach is applicable.

As mentioned above, in order to demonstrate how the developed approach works we consider proton scattering on alkali atoms of lithium, sodium, and potassium. These atomic targets contain a single valence electron well isolated from the inner electronic shells. This fact is suggestive to consider the target atom with one active electron in the field of the frozen core. Several previous theoretical approaches used this approximation but they were only able to account for processes involving the electron from the outermost shell. Typically,

these approaches have built on methods proven to successfully generate results that are in good agreement with experimental data for proton collisions with H atoms.

The remaining sections of this paper can be outlined as follows: Section II describes the procedure which is used to treat the electronic structure of multielectron atoms (ions) with a quasi-one-electron configuration. The procedure reduces the target to an effectively one-electron atom. Here we also briefly recapitulate the formalism developed for proton-hydrogen collisions, as well as discuss modifications required for that work so it could be used here. The details of calculations and the obtained results are given in Sec. III. Finally, concluding remarks are given in Sec. IV.

II. FORMALISM

Before looking at collision processes we focus our attention on the description of multielectron targets. The formalism described below is limited to quasi-one-electron (alkali atoms and alkali-like ions) and quasi-two-electron (helium atom, heliumlike ions, alkaline-earth atoms, and alkaline-earth-like ions) targets with one or two electrons in their valence shell. In addition, in this work we consider fully stripped projectiles. The wave-packet continuum discretization for hydrogen-like ions is described in Ref. [55].

A. Target description

In the description of an N -electron target atom with the nuclear charge $Z_T = N$ we adopt the following conventions. The spatial coordinate and the spin of one particular electron are denoted by \mathbf{r} and s , respectively. For convenience, we call this electron an active electron, although, as will become clear below, any one of the remaining $N - 1$ electrons could also be taken as an active electron. An ensemble of $N - 1$ spatial coordinates of the remaining $N - 1$ electrons is denoted by \mathbf{r}' and their spins by s' . The target wave function satisfies the following multielectron Schrödinger equation:

$$[H_T - E_T]\Phi(\mathbf{r}, \mathbf{r}', s, s') = 0, \quad (1)$$

where E_T is the target state energy and

$$H_T = -\frac{1}{2}\nabla_r^2 - \frac{1}{2}\nabla_{r'}^2 + V \quad (2)$$

is the full nonrelativistic target Hamiltonian. Here $-\nabla_r^2/2$ represents the kinetic-energy operator of the active electron while $-\nabla_{r'}^2/2$ is just a short-hand notation for the sum of the kinetic-energy operators of the remaining $N - 1$ electrons, i.e.,

$$-\frac{1}{2}\nabla_{r'}^2 \equiv -\frac{1}{2}\sum_{i=1}^{N-1}\nabla_{r_i}^2. \quad (3)$$

The total interaction potential is given as

$$V = -\sum_{i=1}^N \frac{Z_T}{r_i} + \sum_{i>j}^N \frac{1}{|r_i - r_j|}, \quad (4)$$

where $\sum_{i>j}^N$ denotes summation over both i and j subject to the condition $i > j$. We neglect spin-orbit interactions.

For a wide range of atomic elements in the periodic table there already exist several approaches to compute the

multielectron wave function $\Phi(\mathbf{r}, \mathbf{r}', s, s')$. One of the most elaborate and readily available methods is the multiconfiguration Hartree-Fock (MCHF) approach. In this work we use the computational atomic structure package based on the MCHF approach developed by Froese-Fischer *et al.* [56]. This package can produce multielectron wave functions for the ground and excited states of practically all the elements in the periodic table. It constructs the total atomic wave function using the configuration state functions, which are found by numerically solving corresponding Hartree-Fock equations. Unlike the methods based on the expansion into the linear combination of Slater orbitals, this package allows us to accurately compute the required configuration state functions for a sufficiently long range of radial distances. This is particularly useful for the purpose of the present work, where we need only the ground-state wave function of a particular atom.

Let us denote the ground-state wave function of the multielectron target as $\Phi_0(\mathbf{r}, \mathbf{r}', s, s')$ and assume it is antisymmetrized as necessary. We also assume that the wave function is normalized:

$$\sum_{s,s'} \int |\Phi_0(\mathbf{r}, \mathbf{r}', s, s')|^2 d\mathbf{r}d\mathbf{r}' = 1. \quad (5)$$

The total multielectron probability density in the ground state is given by $|\Phi_0(\mathbf{r}, \mathbf{r}', s, s')|^2$. If we integrate the total electron density over all variables except for the spatial variable of the active electron, then we get the single-electron density

$$\sum_{s,s'} \int |\Phi_0(\mathbf{r}, \mathbf{r}', s, s')|^2 d\mathbf{r}' = \rho(\mathbf{r}). \quad (6)$$

This single-electron density function effectively represents the probability density of finding the active electron at position \mathbf{r} from the target nucleus. Accordingly,

$$\int \rho(\mathbf{r})d\mathbf{r} = 1. \quad (7)$$

Equation (6) can be written as

$$\sum_{s,s'} \int n(\mathbf{r}, \mathbf{r}', s, s')d\mathbf{r}' = 1, \quad (8)$$

where we introduced the following notation:

$$n(\mathbf{r}, \mathbf{r}', s, s') \equiv \frac{|\Phi_0(\mathbf{r}, \mathbf{r}', s, s')|^2}{\rho(\mathbf{r})}. \quad (9)$$

Note that the latter parametrically depends on the position of the active electron. Now we assume that there are single-electron and multielectron wave functions that respectively define the aforementioned single-electron and multielectron probability densities, i.e.,

$$\rho(\mathbf{r}) = |\varphi_0(\mathbf{r})|^2, \quad (10)$$

$$n(\mathbf{r}, \mathbf{r}', s, s') = |\phi_0(\mathbf{r}, \mathbf{r}', s, s')|^2. \quad (11)$$

Then we can write the target wave function in the following form:

$$\Phi_0(\mathbf{r}, \mathbf{r}', s, s') = \varphi_0(\mathbf{r})\phi_0(\mathbf{r}, \mathbf{r}', s, s'). \quad (12)$$

Thus, $\varphi_0(\mathbf{r})$ is an effective single-electron wave function and $\phi_0(\mathbf{r}, \mathbf{r}', s, s')$ is an effective $N - 1$ electron wave function

that parametrically depends on \mathbf{r} , the position of the active electron. Due to Eqs. (5), (7), and (8) all three wave functions involved in Eq. (12) are normalized to 1. Moreover, the normalization condition (8) holds for any \mathbf{r} . This imposes a constraint on the functional dependence of $\phi_0(\mathbf{r}, \mathbf{r}', s, s')$ on \mathbf{r} .

Inserting the target wave function written in the factorized form (12) into Eq. (1) leads to

$$\begin{aligned} & -\phi_0(\mathbf{r}, \mathbf{r}', s, s') \frac{1}{2} \nabla_r^2 \phi_0(\mathbf{r}) + \phi_0(\mathbf{r}) H_T \phi_0(\mathbf{r}, \mathbf{r}', s, s') \\ & - \nabla_r \phi_0(\mathbf{r}) \nabla_r \phi_0(\mathbf{r}, \mathbf{r}', s, s') - E_T \phi_0(\mathbf{r}) \phi_0(\mathbf{r}, \mathbf{r}', s, s') \\ & = 0. \end{aligned} \quad (13)$$

Now we write the target state energy E_T as a sum of the core electron energy, ε_c , and the energy of the active electron, ε_0 , i.e.,

$$E_T = \varepsilon_c + \varepsilon_0. \quad (14)$$

Next we multiply Eq. (13) by $\phi_0^*(\mathbf{r}, \mathbf{r}', s, s')$ from the left and integrate over $d\mathbf{r}'$ and sum over spins s and s' , taking into account the normalization condition (8). This leads to

$$-\frac{1}{2} \nabla_r^2 \phi_0(\mathbf{r}) + U(\mathbf{r}) \phi_0(\mathbf{r}) - G(\mathbf{r}) \nabla_r \phi_0(\mathbf{r}) = \varepsilon_0 \phi_0(\mathbf{r}), \quad (15)$$

where we introduced the following short-hand notation:

$$U(\mathbf{r}) = \sum_{s,s'} \int \phi_0^*(\mathbf{r}, \mathbf{r}', s, s') (H_T - \varepsilon_c) \phi_0(\mathbf{r}, \mathbf{r}', s, s') d\mathbf{r}', \quad (16)$$

and

$$G(\mathbf{r}) = \sum_{s,s'} \int \phi_0^*(\mathbf{r}, \mathbf{r}', s, s') \nabla_r \phi_0(\mathbf{r}, \mathbf{r}', s, s') d\mathbf{r}'. \quad (17)$$

The quantity $U(\mathbf{r})$ is an expectation value of the full-target Hamiltonian H_T over the spatial coordinates of the $N - 1$ electrons and the spin space of all N electrons. It represents the collective field produced by the target nucleus and all the target electrons except for the active electron. It takes into account the possibility of excitations of not only the outermost electron but also the electrons from the inner shells and has a very different meaning than effective potentials commonly used in DFT. Therefore, to avoid confusion with the usual effective potential, we call $U(\mathbf{r})$ a pseudopotential. As we see below, our pseudopotential has very different functional behavior than traditional effective potentials.

In the present work we employ the multiconfiguration Hartree-Fock approach according to which

$$\rho(\mathbf{r}) = |\phi_0(\mathbf{r})|^2 = \frac{\sum_{i=1}^{\nu} \omega_i |\psi_i(\mathbf{r})|^2}{N}, \quad (18)$$

where ν is the total number of configurations in the ground state of the atom, and ω_i is the occupation number of the electrons in the configuration state $\psi_i(\mathbf{r})$. The configuration state functions $\psi_i(\mathbf{r})$ are obtained using the same computational atomic structure package [56]. For the quasi-one-electron and quasi-two-electron atoms considered in this work all configuration state functions are s -wave ones. Therefore, the multielectron wave function $\Phi_0(\mathbf{r}, \mathbf{r}', s, s')$ and its components $\phi_0(\mathbf{r})$ and $\phi_0(\mathbf{r}, \mathbf{r}', s, s')$ are all real functions. Therefore,

we can write

$$\begin{aligned} G(\mathbf{r}) &= \sum_{s,s'} \int \phi_0(\mathbf{r}, \mathbf{r}', s, s') \nabla_r \phi_0(\mathbf{r}, \mathbf{r}', s, s') d\mathbf{r}' \\ &= \frac{1}{2} \nabla_r \sum_{s,s'} \int \phi_0(\mathbf{r}, \mathbf{r}', s, s') \phi_0(\mathbf{r}, \mathbf{r}', s, s') d\mathbf{r}' \\ &= \frac{1}{2} \nabla_r \sum_{s,s'} \int n(\mathbf{r}, \mathbf{r}', s, s') d\mathbf{r}' = 0. \end{aligned} \quad (19)$$

Above we took into account Eq. (8).

Thus, Eq. (15) reduces to the following effective one-electron Schrödinger equation:

$$-\frac{1}{2} \nabla_r^2 \phi_0(\mathbf{r}) + U(\mathbf{r}) \phi_0(\mathbf{r}) = \varepsilon_0 \phi_0(\mathbf{r}). \quad (20)$$

Since in our case the solution of this equation $\phi_0(\mathbf{r})$ does not depend on the solid angle $\hat{\mathbf{r}}$, this indicates that the pseudopotential is spherically symmetric. Hence, we arrive at the following effective one-electron radial Schrödinger equation:

$$\left[-\frac{1}{2} \frac{d^2}{dr^2} - \frac{1}{r} \frac{d}{dr} + U(r) \right] \phi_0(r) = \varepsilon_0 \phi_0(r). \quad (21)$$

One should note that the ground-state wave function ϕ_0 does not represent the state of the isolated valence electron. Rather, it reflects the state of any one of the electrons of the atom in the field of pseudopotential $U(r)$. In other words the multi-electron atom with inner and outer electrons is modeled as a one-electron pseudo-atom.

To compute the pseudopotential $U(r)$ we first need to calculate $\phi_0(r)$. For the atoms considered in this work, the radial probability density $\rho(r)$ is a nodeless function, hence its positive square root defines $\phi_0(r)$. In Fig. 1(a) we present the ground-state radial wave function $\phi_0(r)$ multiplied by r for the Li, Na, and K atoms. Here one can see features reflecting the electronic structure of the corresponding targets: a number of maxima are observed, each representing localized positions of shell electrons. This is because these wave functions are obtained by taking the square root from the probability density functions as in Eq. (10). As one can see, all presented wave functions are nodeless, therefore there is no difficulty in obtaining the wave function from the probability density function.

Once $\phi_0(r)$ is obtained the pseudopotential $U(r)$ is found by reverse solving Eq. (21), i.e.,

$$U(r) = \varepsilon_0 + \frac{1}{\phi_0(r)} \left[\frac{1}{2} \frac{d^2}{dr^2} + \frac{1}{r} \frac{d}{dr} \right] \phi_0(r). \quad (22)$$

The value of ε_0 is found by ensuring that the $U(r)$ becomes $-1/r$ in the asymptotic limit $r \rightarrow \infty$. The results obtained are then verified against the values of $U(r)$ computed directly using Eq. (16). In Fig. 1(b) we present the radial dependence of the pseudopotential $U(r)$ multiplied by r for the Li, Na, and K atoms. Here $U(r)$ is the potential which is felt by any one of the electrons in the field produced by the nucleus and the remaining electrons of the atom. We infer from the figure that for all three atoms the pseudopotential tends to the expected functional form of $-Z_T/r$ near the origin and has the asymptotic $-1/r$ tail at large distances. Generally, the pseudopotential is attractive except in the intermediate

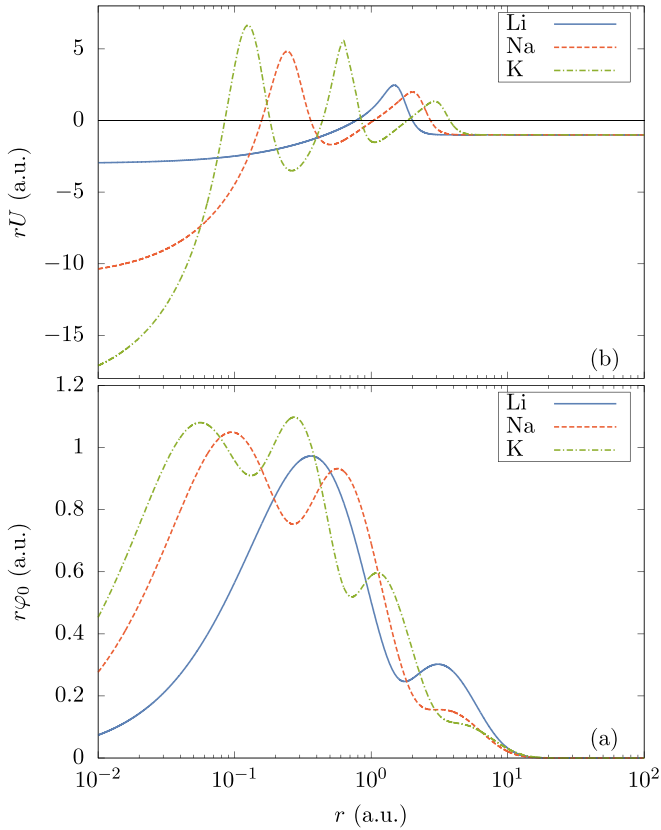


FIG. 1. The ground-state radial wave function $\varphi_0(r)$ [panel (a)] and pseudopotential $U(r)$ [panel (b)] weighted by radius r as functions of r for the Li, Na, and K atoms.

region where one can see an oscillatory behavior. This is consistent with the electronic structure of the considered atoms. In particular, for the Li atom with the $1s^2 2s^1$ electronic configuration there is a region around 1.42 a.u. where the pseudopotential becomes repulsive. This is due to the occupied $n = 1$ shell. The states in this shell are on average either unavailable or unlikely to be available for the active electron. Similarly, for the Na atom with the $1s^2 2s^2 2p^6 3s^1$ electronic configuration there are two regions, one around 0.23 a.u. and the other around 1.94 a.u., where the potential is positive. The first peak is due to the complete $n = 1$ shell and the second is due to the $n = 2$ shell. For the K atom with the $1s^2 2s^2 2p^6 3s^2 3p^6 4s^1$ electronic configuration there are three regions (located around 0.12, 0.62, and 2.83 a.u.) where the pseudopotential turns repulsive, corresponding to the complete $n = 1$, $n = 2$, and $n = 3$ shells, respectively. It is noteworthy to mention that no such oscillatory features in the intermediate region are observed in the model effective potential proposed by Klapisch [46] and employed in proton-alkali atom scattering calculations by Lühr and Saenz [45]. The Klapisch potential based on multiple tuning parameters accurately reproduces the $-Z_T/r$ behavior near the origin and the asymptotic $-1/r$ tail. However, it goes from one functional behavior to the other smoothly and monotonically. Our pseudopotentials appear to better reflect the physical situation that the active electron should experience.

The presently calculated ionization potentials of the ground-state Li, Na, and K atoms, $|\varepsilon_0|$, are 5.34, 4.96, and 4.21 eV, respectively. They compare favorably to the corresponding experimentally measured values of 5.39, 5.14, and 4.34 eV, respectively. This level of agreement with experiment is consistent with the underlying multiconfiguration Hartree-Fock approach used in the current model.

The radial wave functions and corresponding energies for other bound and continuum states of the multielectron atom are found by solving the following reduced radial single-electron Schrödinger equation for each angular momentum l :

$$\left[-\frac{1}{2} \frac{d^2}{dr^2} - \frac{1}{r} \frac{d}{dr} + \frac{l(l+1)}{2r^2} + U(r) \right] R_\alpha(r) = \varepsilon_\alpha R_\alpha(r), \quad (23)$$

where index α denotes the set of quantum numbers specifying an atomic state. Specifically, $\alpha = \{nl\}$ for a bound state ($\varepsilon_\alpha < 0$) and $\alpha = \{\kappa l\}$ for the continuum ($\varepsilon_\alpha > 0$), where $\kappa = \sqrt{\varepsilon_\alpha}$. The pseudopotential $U(r)$ is the one that results from reverse solving Eq. (21) for a given $\varphi_0(r)$. Equation (23) is solved using the Numerov method. The bound states are found by utilizing a standard shooting method. The resulting states form a set of negative-energy pseudostates approximately representing the target space, including the ground state. The latter, of course, coincides with $\varphi_0(r)$ and is accurate by construction. For the continuum states, $R_\alpha(r)$ is matched to the Coulomb function at large r , which is also used to derive the continuum phase shift η_l . The radial functions for the bound states are normalized. The continuum wave function is normalized to the δ function in momentum space.

Unlike bound states, which only exist at discrete levels of the target energy spectrum, continuum states can be generated by solving Eq. (23) for arbitrary electron ejection energies. However, the non-normalizable nature of the atomic continuum wave function makes it inapplicable for close-coupling scattering models. To overcome this problem while keeping the flexibility of generating a state for arbitrary continuum energies, we use the wave-packet continuum-discretization approach, which was recently applied to describe the structure of atomic hydrogen [55]. To construct normalizable wave packets, we first take the continuous spectrum of the active electron with some maximum value of energy E_{\max} , and then subdivide the entire interval $[0, E_{\max}]$ into N_c nonoverlapping but touching intervals (discretization bins) $[\varepsilon_{i-1}, \varepsilon_i]_{i=1}^{N_c}$ with $\varepsilon_0 = 0$ and $\varepsilon_{N_c} = E_{\max}$. Every such energy bin corresponds to the interval $[\kappa_{i-1}, \kappa_i]$ in momentum space, where $\kappa_i = \sqrt{\varepsilon_i}$. The wave packet (WP) corresponding to each bin is built from the following integral of the continuum function [which is the solution of Eq. (23)]:

$$R_{il}^{\text{WP}}(r) = \int_{\kappa_{i-1}}^{\kappa_i} d\kappa R_{\kappa l}(r). \quad (24)$$

Then the reduced target atom wave function is defined as

$$\varphi_\alpha^{\text{WP}}(\mathbf{r}) = R_{n_\alpha l_\alpha}^{\text{WP}}(r) Y_{l_\alpha m_\alpha}(\hat{\mathbf{r}}), \quad (25)$$

where Y_{lm} denote the spherical harmonics. As mentioned above, the continuum functions are normalized to the δ function. This condition ensures the orthogonality and

normalization of the wave-packet pseudostates,

$$\langle \varphi_{\alpha'}^{\text{WP}} | \varphi_{\alpha}^{\text{WP}} \rangle = \delta_{\alpha'\alpha}. \quad (26)$$

For a particular angular momentum l , N_c wave-packet pseudostates representing the $[0, E_{\text{max}}]$ region of the active electron continuum, together with N_b bound states, form a practically complete set of pseudostates, provided N_c and N_b are sufficiently large. For the given maximum allowed angular momentum l_{max} , the total number of channels becomes $N = \sum_{l=0}^{l_{\text{max}}} (2l+1)(N_b - l + N_c)$. The number of negative- and positive-energy states, as well as E_{max} , are increased until adequate convergence is achieved in the predicted cross sections for the collision process that we are interested in.

B. Scattering equations

With the description of the multielectron target effectively as a one-electron atom we can now apply the formalism developed for proton-hydrogen collisions [22,57]. The total scattering wave function can be expanded using the projectile and target bases. The projectile basis describes the proton-active electron system, and, therefore, consists of hydrogen eigenstates and hydrogen continuum wave-packet pseudostates. The details of the basis describing atomic hydrogen are given in Ref. [55]. Consequently, the Schrödinger equation is expressed as a system of differential equations for unknown time-dependent expansion coefficients. In the asymptotic region these time-dependent coefficients represent the transition amplitudes for all processes including elastic scattering, excitation, ionization, and electron capture depending on the final-state energy and the electron arrangement.

We gave extended details of the wave-packet convergent close-coupling (WP-CCC) approach in our previous studies of proton-hydrogen collisions [22,57]. Its extension to the four-body proton-helium problems is presented in Ref. [25]. Here we generalize this approach to proton collisions with multielectron atomic targets.

In the previous section we derived the procedure which reduces the description of the multielectron atom to the effectively two-body system consisting of a core ion and one active electron. The mutual interaction of electrons, the electron-exchange effects and the interaction of multiple electrons with the atomic nucleus are all represented by one active electron and the core ion. With this description of the target, the collision system reduces to an effectively three-body scattering problem. Therefore, we can apply our existing WP-CCC approach with slight modifications which involve only introducing pseudopotentials representing interactions of the target core ion with the active electron and the incident proton. Scattering of the projectile with the target described by the procedure derived above is governed by the following effective three-body Schrödinger equation for the total scattering wave function Ψ_i^+ :

$$(H - E)\Psi_i^+ = 0, \quad (27)$$

with the outgoing-wave boundary conditions. Here E denotes the total energy and H denotes the Hamiltonian for the system of the projectile, the target core ion, and the active electron. The initial channel is denoted with index i and the total scattering wave function develops from that state. We look for

the solution to Eq. (27) in the form of an expansion of Ψ_i^+ in a two-center basis of the target (φ_{α}) and projectile (φ_{β}) pseudostates as

$$\Psi_i^+ \approx \sum_{\alpha=1}^{N_T} F_{\alpha}(t, \mathbf{b}) \varphi_{\alpha}(\mathbf{r}_T) e^{i\mathbf{q}_{\alpha} \cdot \boldsymbol{\rho}} + \sum_{\beta=1}^{N_P} G_{\beta}(t, \mathbf{b}) \varphi_{\beta}(\mathbf{r}_P) e^{i\mathbf{q}_{\beta} \cdot \boldsymbol{\sigma}}, \quad (28)$$

where F_{α} and G_{β} are expansion coefficients, and the numbers of target and projectile basis functions are denoted with N_T and N_P , respectively. We use the Jacobi coordinates. Here, index α denotes a quantum state in a channel where the projectile with relative momentum \mathbf{q}_{α} is incident on target bound state α . A quantum state in the rearrangement channel, where the electron is transferred to state β of the atom formed by the projectile has momentum \mathbf{q}_{β} relative to the target nucleus is denoted with index β . Vector $\boldsymbol{\rho}$ denotes the position of the projectile relative to the center of mass of the residual target ion-active electron system. The position of the projectile-active electron system relative to the residual target ion is denoted as $\boldsymbol{\sigma}$. The position of the projectile with respect to the residual target ion is denoted as \mathbf{R} . If we introduce impact parameter \mathbf{b} , then we can write $\mathbf{R} = \mathbf{b} + \mathbf{v}t$, where \mathbf{v} denotes the velocity of the projectile. Vector \mathbf{r}_T denotes the position of the active electron relative to the target proton. the position of the active electron relative to the projectile is denoted as \mathbf{r}_P .

The set of basis states representing the H atom formed when the projectile captures the electron is made of the eigenstates corresponding to the H bound states and wave packets corresponding to positive-energy bin states [22]. The basis of target atom pseudostates is derived in the previous section. Each of the sets of the target and projectile basis functions are separately orthonormal. We emphasize that the CCC approach is based on a different ansatz for Ψ_i^+ than the traditional close-coupling method (see, e.g., Ref. [58]). The wave function given in Eq. (28) does not satisfy the semiclassical Schrödinger equation. Therefore, we start from the exact Schrödinger equation. However, subsequently, by using the semiclassical approximation, we arrive at the same set of equations for the expansion coefficients as that obtained in the conventional close-coupling approach [58]. This is one of the subtle differences between our approach and the conventional atomic orbital close-coupling ones. See Ref. [22] for details.

It is worthwhile to emphasize the distinguishing features of the present model from the approaches which are based on the independent event model. In Eq. (28) the ground state of the target $\varphi_{\alpha=1}(\mathbf{r}_T) \equiv \varphi_0(\mathbf{r}_T) = \varphi_0(r_T)Y_{00}(\hat{\mathbf{r}}_T)$ is obtained from the probability density function given in Eq. (18), which contains all necessary information about the electrons in every subshell of the target. Additionally, all other target pseudostates of the expansion (28) also contain similar information since they are obtained using the same pseudopotential which was constructed to describe the ground state of the multielectron target. For this very reason the present approach is capable of describing the fate of any one of the target electrons on an equal footing. In contrast, the models which are based on the independent electron approximation treat the target atom as if it has a frozen core and one electron (which is in the outermost shell of the atom), where the interaction potential between them represents the collective field of all electrons in

the frozen core. Therefore, the pseudostates representing the active electron in those models by construction describe only the fate of the electron in the outermost shell of the target.

With the expansion (28) and using the semiclassical approximation, the Schrödinger equation (27) can be expressed as a system of the following first-order differential equations:

$$\begin{cases} i\dot{F}_{\alpha'} + i \sum_{\beta=1}^{N_p} \dot{G}_{\beta} \tilde{K}_{\alpha'\beta} = \sum_{\alpha=1}^{N_T} F_{\alpha} D_{\alpha'\alpha} + \sum_{\beta=1}^{N_p} G_{\beta} \tilde{Q}_{\alpha'\beta}, \\ i \sum_{\alpha=1}^{N_T} \dot{F}_{\alpha} K_{\beta'\alpha} + i\dot{G}_{\beta'} = \sum_{\alpha=1}^{N_T} F_{\alpha} Q_{\beta'\alpha} + \sum_{\beta=1}^{N_p} G_{\beta} \tilde{D}_{\beta'\beta}, \\ \alpha' = 1, 2, \dots, N_T, \quad \beta' = 1, 2, \dots, N_p, \end{cases} \quad (29)$$

where time derivatives are denoted with dots over F_{α} and F_{β} . Overlap integrals $K_{\beta'\alpha}$ are written as

$$K_{\beta'\alpha}(\mathbf{R}) = \langle \varphi_{\beta'} | \exp[-i\mathbf{v} \cdot \mathbf{r}_T] | \varphi_{\alpha} \rangle \times \exp[iv^2 t/2 + i(\varepsilon_{\beta'} - \varepsilon_{\alpha})t], \quad (30)$$

$$\tilde{K}_{\alpha'\beta}(\mathbf{R}) = \langle \varphi_{\alpha'} | \exp[i\mathbf{v} \cdot \mathbf{r}_T] | \varphi_{\beta} \rangle \times \exp[-iv^2 t/2 + i(\varepsilon_{\alpha'} - \varepsilon_{\beta})t]. \quad (31)$$

Here the energy of the target atom in state α is denoted as ε_{α} , while the energy of the H atom formed in state β after electron transfer is denoted as ε_{β} . Matrix elements $D_{\alpha'\alpha}$ representing direct scattering are given as

$$D_{\alpha'\alpha}(\mathbf{R}) = \langle \varphi_{\alpha'} | \bar{V}_{\alpha} | \varphi_{\alpha} \rangle \exp[i(\varepsilon_{\alpha'} - \varepsilon_{\alpha})t], \quad (32)$$

$$\tilde{D}_{\beta'\beta}(\mathbf{R}) = \langle \varphi_{\beta'} | \bar{V}_{\beta} | \varphi_{\beta} \rangle \exp[i(\varepsilon_{\beta'} - \varepsilon_{\beta})t], \quad (33)$$

where $\bar{V}_{\alpha} = Z_T/R - 1/r_p$ and $\bar{V}_{\beta} = Z_T/R + U(r_T)$. Matrix elements $Q_{\beta'\alpha}$ corresponding to electron capture are written as

$$Q_{\beta'\alpha}(\mathbf{R}) = \langle \varphi_{\beta'} | \exp[-i\mathbf{v} \cdot \mathbf{r}_T] (H_{\alpha} + \bar{V}_{\alpha} - \varepsilon_{\alpha}) | \varphi_{\alpha} \rangle \times \exp[iv^2 t/2 + i(\varepsilon_{\beta'} - \varepsilon_{\alpha})t], \quad (34)$$

$$\tilde{Q}_{\alpha'\beta}(\mathbf{R}) = \langle \varphi_{\alpha'} | \exp[i\mathbf{v} \cdot \mathbf{r}_T] (H_{\beta} + \bar{V}_{\beta} - \varepsilon_{\beta}) | \varphi_{\beta} \rangle \times \exp[-iv^2 t/2 + i(\varepsilon_{\alpha'} - \varepsilon_{\beta})t], \quad (35)$$

where H_{α} and H_{β} are the target (effective) and projectile atom Hamiltonians. In this work they are defined as

$$H_{\alpha} = -\frac{1}{2}\nabla_{r_T}^2 + U(r_T), \quad (36)$$

$$H_{\beta} = -\frac{1}{2}\nabla_{r_p}^2 - \frac{1}{r_p}. \quad (37)$$

We note that Eqs. (29)–(35) are identical to the corresponding equations emerging in the conventional semiclassical approach if the plane-wave electron translational factors are used [21]. The complete details of these derivations can be found in Ref. [22].

At $t \rightarrow \infty$ the time-dependent coefficients $F_{\alpha}(t, \mathbf{b})$ and $G_{\beta}(t, \mathbf{b})$ describe the impact-parameter amplitudes for transitions into the various excited states of the target and projectile-electron system. At $t \rightarrow -\infty$ the following initial

boundary conditions are satisfied:

$$\begin{cases} F_{\alpha}(-\infty, \mathbf{b}) = \delta_{\alpha 1}, & \alpha = 1, 2, \dots, N_T, \\ G_{\beta}(-\infty, \mathbf{b}) = 0, & \beta = 1, 2, \dots, N_p. \end{cases} \quad (38)$$

The calculation details of the direct-scattering and rearrangement matrix elements are described in Ref. [20].

Once the set of differential equations (29) are solved, the cross sections for the individual direct-scattering (denoted as di) and electron-capture (denoted as ec) transitions can be found as

$$\sigma_{\alpha}^{\text{di}} = 2\pi \int_0^{\infty} db b P_{\alpha}^{\text{di}}(b), \quad (39)$$

$$\sigma_{\beta}^{\text{ec}} = 2\pi \int_0^{\infty} db b P_{\beta}^{\text{ec}}(b), \quad (40)$$

respectively, where the transition probabilities are

$$P_{\alpha}^{\text{di}}(b) = N |F_{\alpha}(+\infty, \mathbf{b}) - \delta_{\alpha 1}|^2, \quad (41)$$

$$P_{\beta}^{\text{ec}}(b) = N |G_{\beta}(+\infty, \mathbf{b})|^2. \quad (42)$$

Here we need to emphasize that since the normalization of the total scattering wave function (28) is conserved to unity throughout the entire collision time from $t \rightarrow -\infty$ to $t \rightarrow \infty$, any one of $|F_{\alpha}(+\infty, \mathbf{b})|^2$ and $|G_{\beta}(+\infty, \mathbf{b})|^2$ can never be greater than 1. In the definition of the transition probabilities [Eqs. (41) and (42)] the factor N indicates that any one of N target electrons can be involved in the transition with an equal probability. Then the total electron-transfer cross section is the combination of all partial cross sections corresponding to the included negative-energy hydrogen states on the projectile center. The total single-ionization cross section is the sum of the partial cross sections for excitation of the pseudostates corresponding to positive energies on the target center and electron transfer into the pseudostates corresponding to the continuum of hydrogen.

III. RESULTS AND DETAILS OF CALCULATIONS

In this section we apply the developed method to calculate the total electron capture and the total ionization cross sections in proton collisions with alkali atoms. An accurate calculation of various collision processes occurring in proton collisions on alkali atoms of Li, Na, and K require a sufficiently large two-center basis of target and projectile pseudostates. The convergence of the results has been investigated by increasing several target and projectile dependent parameters. The parameters which are tested in convergence studies are the maximum orbital quantum number l_{max} , the number N_b of bound (negative-energy) states and the number N_c of continuum bin states per orbital angular momentum l . Also, we verify that the maximum energy E_{max} of the electron continuum covered by wave-packet bins is sufficiently large. For all incident energies of the projectile studied in this work the two-center basis with $l_{\text{max}} = 4$, $N_b = 5 - l$, $E_{\text{max}} = 400$ eV, and $N_c = 20$ is found to be sufficient. Thus, the total number of projectile and target channels is 2×555 . This allows one to calculate the total single-electron transfer and total single-ionization cross sections with acceptable accuracy. Also, during the solution of the set of differential equations

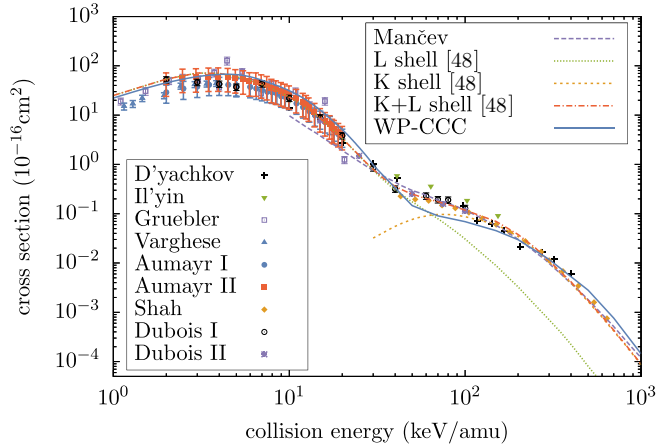


FIG. 2. Total cross section for single electron transfer in p -Li collisions. The results of the present WP-CCC approach are shown in comparison with the experimental data by D'yachkov [26], Il'in *et al.* [27], Gruebler *et al.* [28], Aumayr *et al.* [29,30], Varghese *et al.* [31], Shah *et al.* [33], DuBois [61], and DuBois and Toburen [34] and theoretical calculations by Mančev *et al.* [62], Labaigt and Dubois [63] and our previous calculations for single-electron capture from the K and L shells of the Li target and the aggregate of capture from the K and L shells [48].

(29) we always make sure that the normalization of the total wave function (28) is 1 at every time step.

In our calculations we found the lowest energy region (1–10 keV) to be the most challenging. In this region we encountered ill-conditioning problems due to norm unity violation. However, these issues have been successfully eliminated by significantly increasing the number of Runge-Kutta time steps (e.g., at 1 keV it had to be increased to 10 000) and the accuracy of the overlap and electron-transfer matrix elements which are computed in spheroidal coordinates. The accuracy of the latter is controlled by increasing the number of integration quadrature points for calculating the transition matrix elements. In the worst case of 1 keV we used 500 points for each spheroidal coordinate. The computational code that solves Eq. (29) runs on GPU-based supercomputers, which reduces the computational time tremendously. We utilize the OpenACC directives of Fortran [59] to offload calculations of direct and rearrangement matrix elements to GPUs. For solving the system of equations which emerge at every step of the Runge-Kutta propagation, we use the CUDA library *cuSolverDn* [60].

In Fig. 2 we show the total single-electron-capture cross section as a function of incident energy in proton-lithium collisions. Our results (the solid line) are displayed in comparison with the experimental data [26–31,33,34,61] and theoretical results of Mančev *et al.* [62] and Labaigt and Dubois [63]. As seen from the figure, agreement with experimental data is good in the entire range of impact energies considered in this work. At the energy region of 30 keV and above, the measured total electron-capture cross sections display a shoulder-like structure. Our previous calculations [48] (represented by the dotted green line) showed that this behavior cannot be explained by taking into account only the capture of the outer $2s$ electron of the target lithium. At high impact

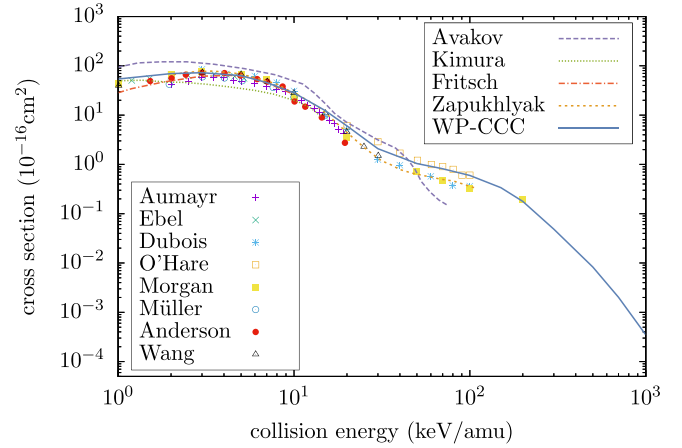


FIG. 3. Total cross section for single-electron transfer in p -Na collisions. The results of the present WP-CCC approach are shown in comparison with the experimental data by Müller *et al.* [32], DuBois and Toburen [34], Aumayr *et al.* [35], Ebel and Salzborn [36], O'Hare *et al.* [37], Morgan *et al.* [38], Anderson *et al.* [39], Wang *et al.* [40], and Zapukhlyak *et al.* [64], and theoretical results by Avakov *et al.* [65], Kimura *et al.* [66], Fritsch [67], and Zapukhlyak *et al.* [64].

energies incident protons can go deeper into the lithium atom and interact with its inner electrons which leads to the capture of K -shell electrons. In our recent work [48] we modeled this process by considering it as a collision of protons with the heliumlike $\text{Li}^+(1s^2)$ target with the charge of 3. That model neglected the effect of the valence L -shell electron. This is a widely used approximation. The sum of the capture cross sections of the L - and K -shell target electrons indeed displayed good agreement with experiment. Analyzing the results one can see that at energies above 100 keV the electron capture from the K shell is significantly more pronounced than that from the L shell. At the same time, at low energies the L -shell electron capture is the main contributor. In a similar way the three-body boundary-corrected continuum intermediate-state (BCIS) method of Mančev *et al.* [62] also considered the capture of K - and L -shell electrons of the lithium target as two independent processes. The BCIS results are in overall good agreement with experimental data at intermediate and high-energy regions. However, due to the perturbative nature of the BCIS method their results are systematically lower than the measured data below 30 keV.

In our present calculations the Li target is treated using a pseudopotential in a way which takes into account the possibility of K - and L -shell electron excitations. Therefore, the final electron-capture cross section already includes their aggregate effect. Also presented are the results of Labaigt and Dubois [63], which are obtained using the semiclassical, nonperturbative approach which takes into account all three electrons of the collision system. We should note that these results are reproduced from Ref. [63] by summing the cross sections representing transfer from the valence and inner electrons. Similar to the present approach these calculations are not based on the independent-event model.

In Figs. 3 and 4 we present our results of the total single-electron capture cross sections for proton collisions on atomic

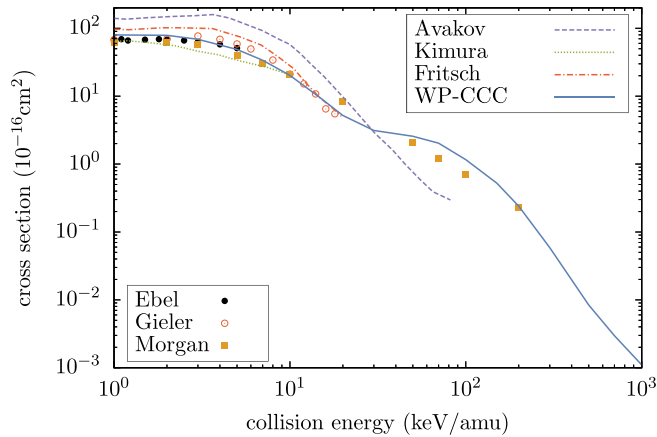


FIG. 4. Total cross section for single-electron transfer in p -K collisions. The results of the present WP-CCC approach are displayed in comparison with the experimental data by Ebel and Salzborn [36], Morgan *et al.* [38], and Gieler *et al.* [41], and theoretical results by Kimura *et al.* [66], Fritsch [67], and Avakov *et al.* [65].

targets targets of Na, and K, respectively. Here also the obtained results are in good agreement with available experimental measurements [32,34–41] across a wide energy range displayed. If considered separately, similarly to the Li case, the contribution of electron capture from the inner shells would dominate over capture from the outermost shell at the incident energies above 30 keV. These figures demonstrate a clear advantage of the present method over the independent-event model. The latter would require combination of the cross sections for three independent events for the Na target and four independent events for the K target. Clearly, the independent-event model becomes very cumbersome and impractical for targets with several shells. In addition, it neglects the effect of coupling between the shells of the target to the final results. Instead the independent-event model introduces several screening parameters corresponding to each target shell. This leads to the final results becoming too sensitive to the choice of these parameters. At the same time we note that the results of Zapukhlyak *et al.* [64] obtained by considering three independent events show good agreement with experiment.

Figure 5 presents the total single-ionization cross section a function of incident energy in proton-lithium collisions. One can see that the obtained results are in excellent agreement with the measurements of Shah *et al.* [33] and DuBois [61], but significantly overestimate the measurements of D'yachkov [26] at collision energies below 70 keV. At the same time, at energies above 100 keV the measurements of D'yachkov [26] are larger than the present calculations and the measurements of Shah *et al.* [33]. One should note that these single-ionization cross sections include also the contribution of inner-shell electrons, as in the case with electron capture. The results of CDW-EIS calculations of McCartney and Crothers [43] are generally lower than the present results and in better agreement with the measurements of D'yachkov [26] at 30 and 40 keV. Measurements of DuBois [61] are for multiple ionization where single ionization is expected to dominate.

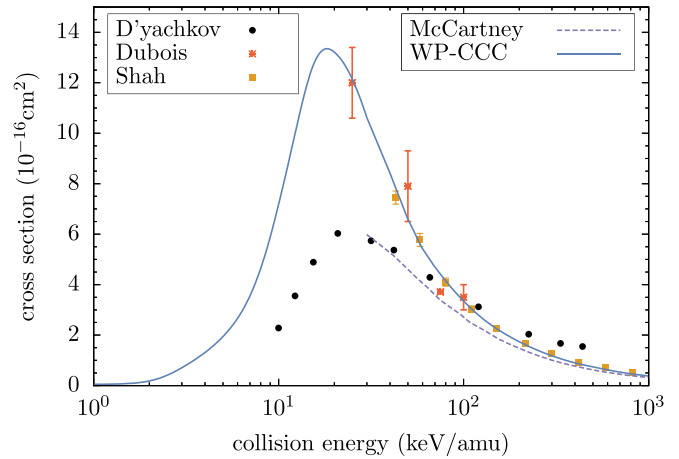


FIG. 5. Total cross section for single ionization in p -Li collisions. The results of the present WP-CCC approach for p -Li collisions are shown in comparison with the experimental data by D'yachkov [26], Shah *et al.* [33], and DuBois [61], and theoretical calculations of McCartney and Crothers [43].

The total single-ionization cross section for p -Na collisions as a function of incident proton energy is shown in Fig. 6. The obtained results for p -Na collisions are in reasonable agreement with the measurements of Zapukhlyak *et al.* [64] but significantly underestimate the measurements of O'Hare *et al.* [37] and DuBois [68]. Again, measurements of DuBois [68] are for multiple ionization. We should also note overall the good agreement of the present results with the classical trajectory Monte Carlo calculations of Lundy and Olson [69]. In general, all the calculations appear to agree in shape but can differ in magnitude up to 60%.

Figure 7 presents the total cross section for single ionization in p -K collisions. Our results disagree with the measurements of O'Hare *et al.* [37] except at 100 keV where

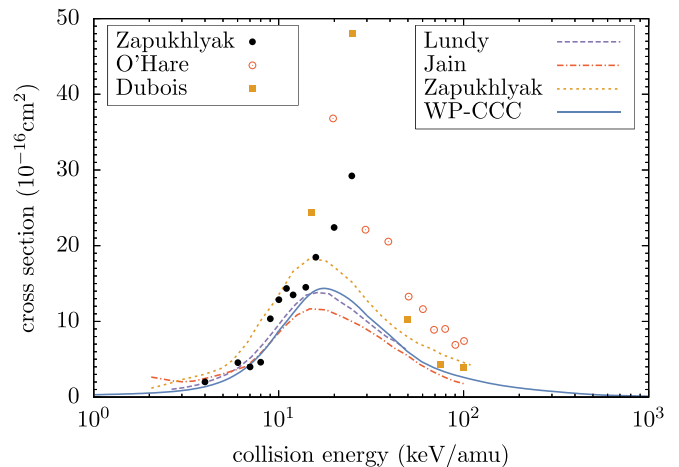


FIG. 6. Total cross section for single ionization in p -Na collisions. The results of the present WP-CCC approach are shown in comparison with the experimental data by O'Hare *et al.* [37], Zapukhlyak *et al.* [64], and DuBois [68] and the theoretical results of Lundy and Olson [69], Jain and Winter [70], and Zapukhlyak *et al.* [64].

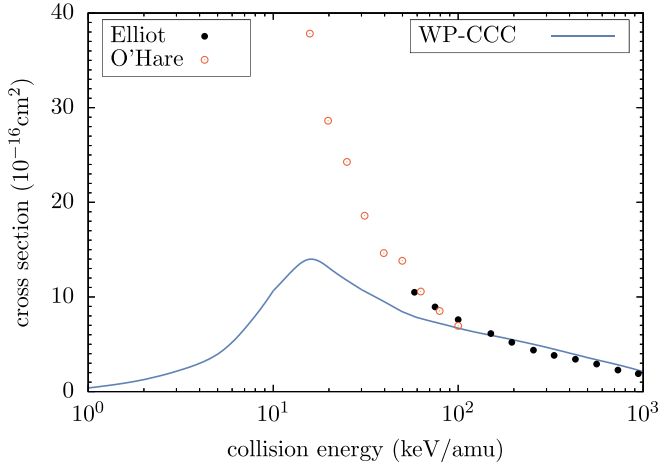


FIG. 7. Total cross section for single ionization in p -K collisions. The results of the present WP-CCC approach are displayed in comparison with the experimental data by Elliott *et al.* [71] and O'Hare *et al.* [37].

they merge. Above 100 keV our results agree well with the measurements of Ref. Elliott *et al.* [71]. To our best knowledge, for the K target there are no other theoretical studies of this process.

Discrepancies between theory and experiment for single ionization of Na and K around the peak region are striking. Zapukhlyak *et al.* [64] speculated that the experimental p -Na ionization cross sections might be higher than the theoretical ones possibly due to contributions from autoionizing doubly excited states, which were ignored in their calculation. Our effective single-electron approach also neglects such contributions. At the same time, Zapukhlyak *et al.* [64] estimated these contributions to be about two orders of magnitude smaller than the net ionization cross section over the whole range of impact energies. Indeed this makes sense. We also notice that the disagreement appears to worsen as the projectile energy falls from 100 down to 20 keV. This is counterintuitive as the likelihood of exciting an inner-shell electron to form an auto-ionizing state should fall with energy. This is because the probability of the projectile penetrating deeper into the target atom is smaller at lower energies. Thus, not only do the discrepancies for single-electron ionization in p -Na collisions above $E = 20$ keV still remain unexplained but a similar issue also exists for p -K collisions. This situation warrants further experimental and theoretical investigations.

IV. CONCLUSIONS

An effective single-electron approach to proton collisions with multielectron atoms is developed. The method allows the calculation of single-ionization and single-electron capture cross sections taking into account the effect of all the inner and outer shell target electrons. The ground-state wave function obtained in the multiconfiguration Hartree-Fock approach is used to calculate the probability density averaged over spins and all the configuration-space variables except for the position of one electron from the nucleus. The obtained single-electron probability density is then used to derive a

pseudopotential describing the interaction of one electron with the collective field produced by the target nucleus and the other electrons. This pseudopotential is also used to construct the effective three-body Schrödinger equation of the scattering system. The total wave function is expanded using a two-center basis built from wave-packet pseudostates. This allows us to convert the Schrödinger equation into a set of coupled differential equations for the expansion coefficients. In the asymptotic region these time-dependent coefficients represent transition amplitudes for all processes including elastic scattering, excitation, ionization, and electron capture. The approach allows calculating single-ionization and single-electron capture cross sections by considering the possibility of excitation of any one of the inner or outer shell target electrons. Accordingly, the approach does not differentiate which one of the many target electrons is captured or ionized. As an illustrative example we have calculated the total cross sections for single ionization and single electron transfer in proton collisions with lithium, sodium, and potassium. The obtained results are in very good accord with available experimental measurements on electron transfer for all three targets, however, considerable disagreement for single ionization of sodium and potassium has been found. The developed method has a clear advantage over the widely used independent-event model.

We emphasize that our effective single-electron approach is an approximation. It is not as rigorous as the time-dependent density-functional theory. We also accentuate that it is not a general-purpose approach at least in its current stage of development. However, our approach can serve a simpler alternative to TDDFT in cases where it is applicable. As demonstrated in this work it works very well for alkali atoms with one valence electron outside closed shells. Recently, we have tested the approach on the proton-helium differential-scattering problem [72]. The results obtained using the effective single-electron approach show very good agreement with the results from the method based on the correlated two-electron description of the helium target. All this indicates that the approach presented here should also work for quasi-one-electron alkali-like ions and quasi-two-electron alkaline-earth atoms and alkaline-earth-like ions with one or two electrons in their valence shell. Applications to such atoms are straightforward and constitute a possible avenue for future research. We are investigating further to see if the effective single-electron approach developed here can be generalized to other types of atomic targets. Transitioning from quasi-one- and quasi-two-electron atoms to atoms with a partially or fully filled valence shell is not straightforward and poses certain challenges. We are currently working on the extension of the method to other noble gas atoms. Whether the approach is suitable for these atoms remains to be seen.

ACKNOWLEDGMENTS

This work was supported by the Australian Research Council, the Pawsey Supercomputer Centre, and the National Computing Infrastructure. C.T.P. acknowledges support through an Australian Government Research Training Program Scholarship. We thank Paul Oxley for useful discussion and for bringing Ref. [61] to our attention.

- [1] K. Heng and R. A. Sunyaev, *Astron. Astrophys.* **481**, 117 (2008).
- [2] R. Hemsworth, H. Decamps, J. Graceffa, B. Schunke, M. Tanaka, M. Dremel, A. Tanga, H. De Esch, F. Geli, J. Milnes *et al.*, *Nucl. Fusion* **49**, 045006 (2009).
- [3] O. Marchuk, *Phys. Scr.* **89**, 114010 (2014).
- [4] Dž. Belkić, *J. Math. Chem.* **47**, 1366 (2010).
- [5] Dž. Belkić, I. Bray, and A. Kadyrov, *State-of-the-Art Reviews on Energetic Ion-Atom and Ion-Molecule Collisions* (World Scientific, Singapore, 2019).
- [6] S. Zou, L. Pichl, M. Kimura, and T. Kato, *Phys. Rev. A* **66**, 042707 (2002).
- [7] N. Toshima, *Phys. Rev. A* **59**, 1981 (1999).
- [8] T. G. Winter, *Phys. Rev. A* **80**, 032701 (2009).
- [9] H. R. J. Walters and C. T. Whelan, *Phys. Rev. A* **92**, 062712 (2015).
- [10] H. Bräuning, R. Trassl, A. Theiß, A. Diehl, E. Salzborn, M. Keim, A. Achenbach, H. J. Lüdde, and T. Kirchner, *J. Phys. B: At., Mol. Opt. Phys.* **38**, 2311 (2005).
- [11] D. R. Schultz, M. R. Strayer, and J. C. Wells, *Phys. Rev. Lett.* **82**, 3976 (1999).
- [12] A. Kołakowska, M. S. Pindzola, and D. R. Schultz, *Phys. Rev. A* **59**, 3588 (1999).
- [13] A. Jorge, J. Suárez, C. Illescas, L. F. Errea, and L. Méndez, *Phys. Rev. A* **94**, 032707 (2016).
- [14] V. D. Rodríguez, C. A. Ramírez, R. D. Rivarola, and J. E. Miraglia, *Phys. Rev. A* **55**, 4201 (1997).
- [15] F. D. Colavecchia, G. Gasaneo, and C. R. Garibotti, *J. Phys. B: At., Mol. Opt. Phys.* **33**, L467 (2000).
- [16] A. B. Voitkiv, B. Najjari, and J. Ullrich, *J. Phys. B: At., Mol. Opt. Phys.* **36**, 2591 (2003).
- [17] R. E. Olson, *J. Phys. B: At. Mol. Phys.* **15**, L163 (1982).
- [18] C. Illescas, B. Pons, and A. Riera, *Phys. Rev. A* **65**, 030703(R) (2002).
- [19] Dž. Belkić, *Quantum Theory of High-Energy Ion-Atom Collisions* (CRC Press, Boca Raton, 2008).
- [20] I. B. Abdurakhmanov, A. S. Kadyrov, S. K. Avazbaev, and I. Bray, *J. Phys. B: At., Mol. Opt. Phys.* **49**, 115203 (2016).
- [21] S. K. Avazbaev, A. S. Kadyrov, I. B. Abdurakhmanov, D. V. Fursa, and I. Bray, *Phys. Rev. A* **93**, 022710 (2016).
- [22] I. B. Abdurakhmanov, J. J. Bailey, A. S. Kadyrov, and I. Bray, *Phys. Rev. A* **97**, 032707 (2018).
- [23] M. Baxter and T. Kirchner, *Phys. Rev. A* **93**, 012502 (2016).
- [24] S. Borbély, X.-M. Tong, S. Nagele, J. Feist, I. Březinová, F. Lackner, L. Nagy, K. Tórkési, and J. Burgdörfer, *Phys. Rev. A* **98**, 012707 (2018).
- [25] S. U. Alladustov, I. B. Abdurakhmanov, A. S. Kadyrov, I. Bray, and K. Bartschat, *Phys. Rev. A* **99**, 052706 (2019).
- [26] B. A. D'yachkov, *Zh. Tekhn. Fiz.* **38**, 1259 (1968).
- [27] R. N. Il'in, V. A. Oparin, E. S. Solov'ev, and N. V. Fedorenko, *Zh. Tekhn. Fiz.* **36**, 1241 (1966).
- [28] W. Grüebler, P. A. Schmelzbach, V. König, and P. Marmier, *Helv. Phys. Acta* **43**, 254 (1970).
- [29] F. Aumayr, M. Fehringer, and H. Winter, *J. Phys. B: At. Mol. Phys.* **17**, 4201 (1984).
- [30] F. Aumayr, G. Lakits, W. Husinsky, and H. Winter, *J. Phys. B: At. Mol. Phys.* **18**, 2493 (1985).
- [31] S. L. Varghese, W. Waggoner, and C. L. Cocke, *Phys. Rev. A* **29**, 2453 (1984).
- [32] U. Müller, H. A. J. Meijer, N. C. R. Holme, M. Kmit, J. H. V. Lauritsen, J. O. P. Pedersen, C. Richter, J. W. Thomsen, N. Andersen, and S. E. Nielsen, *Z. Phys. D At. Mol. Clust.* **33**, 187 (1995).
- [33] M. B. Shah, D. S. Elliott, and H. B. Gilbody, *J. Phys. B: At. Mol. Phys.* **18**, 4245 (1985).
- [34] R. D. DuBois and L. H. Toburen, *Phys. Rev. A* **31**, 3603 (1985).
- [35] F. Aumayr, G. Lakits, and H. Winter, *J. Phys. B: At. Mol. Phys.* **20**, 2025 (1987).
- [36] F. Ebel and E. Salzborn, *J. Phys. B: At. Mol. Phys.* **20**, 4531 (1987).
- [37] B. G. O'Hare, R. W. McCullough, and H. B. Gilbody, *J. Phys. B: At. Mol. Phys.* **8**, 2968 (1975).
- [38] T. J. Morgan, R. E. Olson, A. S. Schlachter, and J. W. Gallagher, *J. Phys. Chem. Ref. Data* **14**, 971 (1985).
- [39] C. Anderson, A. Howald, and L. Anderson, *Nucl. Instrum. Methods* **165**, 583 (1979).
- [40] Z. Wang, M. Li, W. Xiang, and D. Fu, *Nucl. Instrum. Methods Phys. Res., Sect. B* **450**, 77 (2019).
- [41] M. Gieler, P. Ziegelwanger, F. Aumayr, H. Winter, and W. Fritsch, *J. Phys. B: At., Mol. Opt. Phys.* **24**, 647 (1991).
- [42] C. Stary, H. J. Ludde, and R. M. Dreizler, *J. Phys. B: At., Mol. Opt. Phys.* **23**, 263 (1990).
- [43] M. McCartney and D. S. F. Crothers, *J. Phys. B: At., Mol. Opt. Phys.* **26**, 4561 (1993).
- [44] A. Dubois, S. E. Nielsen, and J. P. Hansen, *J. Phys. B: At., Mol. Opt. Phys.* **26**, 705 (1993).
- [45] A. Lühr and A. Saenz, *Phys. Rev. A* **77**, 052713 (2008).
- [46] M. Klapisch, *Comput. Phys. Commun.* **2**, 239 (1971).
- [47] M. S. Pindzola, T. G. Lee, and J. Colgan, *J. Phys. B: At., Mol. Opt. Phys.* **44**, 205204 (2011).
- [48] I. B. Abdurakhmanov, C. T. Plowman, A. S. Kadyrov, I. Bray, and A. M. Mukhamedzhanov, *J. Phys. B: At., Mol. Opt. Phys.* **53**, 145201 (2020).
- [49] T. Kirchner, H. J. Lüdde, and M. Horbatsch, *Recent Res. Devel. Phys.* **5**, 433 (2004).
- [50] F. Wang, K. Zhang, F. Mao, and J. Wang, *Chem. Phys.* **541**, 111035 (2021).
- [51] X. Hong, F. Wang, Y. Jiao, W. Su, J. Wang, and B. Gou, *J. Chem. Phys.* **139**, 084321 (2013).
- [52] X. Hong, F. Wang, Y. Wu, B. Gou, and J. Wang, *Phys. Rev. A* **93**, 062706 (2016).
- [53] W. Yu, C.-Z. Gao, Y. Zhang, F. S. Zhang, R. Hutton, Y. Zou, and B. Wei, *Phys. Rev. A* **97**, 032706 (2018).
- [54] W. Yu, C.-Z. Gao, S. A. Sato, A. Castro, A. Rubio, and B. Wei, *Phys. Rev. A* **103**, 032816 (2021).
- [55] I. B. Abdurakhmanov, A. S. Kadyrov, and I. Bray, *Phys. Rev. A* **94**, 022703 (2016).
- [56] C. Froese-Fischer, T. Brage, and P. Jönsson, *Computational Atomic Structure: An MCHF Approach* (Taylor & Francis, Boca Raton, 1997).
- [57] I. B. Abdurakhmanov, S. U. Alladustov, J. J. Bailey, A. S. Kadyrov, and I. Bray, *Plasma Phys. Control. Fusion* **60**, 095009 (2018).
- [58] B. H. Bransden and M. R. C. McDowell, *Charge Exchange and the Theory of Ion-Atom Collisions* (Clarendon Press, Oxford, 1992).
- [59] S. Chandrasekaran and G. Juckeland, *OpenACC for Programmers: Concepts and Strategies* (Addison-Wesley Professional, Boston, 2017).

- [60] *cuSolver Library* (NVIDIA Corporation, Santa Clara, 2020).
- [61] R. D. DuBois, *Phys. Rev. A* **32**, 3319 (1985).
- [62] I. Mančev, N. Milojević, D. Delibašić, and Dž. Belkić, *Phys. Scr.* **95**, 065403 (2020).
- [63] G. Labaigt and A. Dubois, *J. Phys.: Conf. Ser.* **488**, 082009 (2014).
- [64] M. Zapukhlyak, T. Kirchner, H. J. Lüdde, S. Knoop, R. Morgenstern, and R. Hoekstra, *J. Phys. B: At., Mol. Opt. Phys.* **38**, 2353 (2005).
- [65] G. V. Avakov, L. D. Blokhintsev, A. S. Kadyrov, and A. M. Mukhamedzhanov, *J. Phys. B: At., Mol. Opt. Phys.* **25**, 213 (1992).
- [66] M. Kimura, R. E. Olson, and J. Pascale, *Phys. Rev. A* **26**, 1138 (1982).
- [67] W. Fritsch, *Phys. Rev. A* **30**, 1135 (1984).
- [68] R. D. DuBois, *Phys. Rev. A* **34**, 2738 (1986).
- [69] C. J. Lundy and R. E. Olson, *J. Phys. B: At., Mol. Opt. Phys.* **29**, 1723 (1996).
- [70] A. Jain and T. G. Winter, *Phys. Rev. A* **51**, 2963 (1995).
- [71] D. S. Elliott, M. B. Shah, and H. B. Gilbody, *J. Phys. B: At. Mol. Phys.* **19**, 3277 (1986).
- [72] K. H. Spicer, C. T. Plowman, I. B. Abdurakhmanov, A. S. Kadyrov, I. Bray, and S. U. Alladustov, *Phys. Rev. A* **104**, 032818 (2021).